PHYSICAL REVIEW B **101**, 125115 (2020)

Reentrant Kondo effect for a quantum impurity coupled to a metal-semiconductor hybrid contact

G. Diniz,[1] G. S. Diniz,[2] G. B. Martins,[1,*] and E. Vernek[1,3]
[1] *Instituto de Física, Universidade Federal de Uberlândia, Uberlândia, Minas Gerais 38400-902, Brazil*
[2] *Curso de Física, Universidade Federal de Jataí, Jataí, GO 75801-615, Brazil*
[3] *Department of Physics and Astronomy, and Nanoscale and Quantum Phenomena Institute, Ohio University, Athens, Ohio 45701-2979, USA*

(Received 7 February 2020; revised manuscript received 29 February 2020; accepted 3 March 2020; published 19 March 2020)

Using the numerical renormalization group (NRG) and Anderson's poor man's scaling, we show that a system containing a quantum impurity (QI), strongly coupled to a semiconductor (with gap 2Δ) and weakly coupled to a metal, displays a *reentrant* Kondo stage as one gradually lowers the temperature T. The NRG analysis of the corresponding single impurity Anderson model (SIAM), through the impurity's thermodynamic and spectral properties, shows that the reentrant stage is characterized by a second sequence of SIAM fixed points, viz., free orbital (FO) → local moment (LM) → strong coupling (SC). In the higher-temperature stage, the SC fixed point (with a Kondo temperature T_{K1}) is unstable, while the lower-temperature Kondo screening exhibits a much lower Kondo temperature T_{K2}, associated to a stable SC fixed point. The results clearly indicate that the reentrant Kondo screening is associated to an effective SIAM, with an effective Hubbard repulsion $U_{\rm eff}$, whose value is clearly identifiable in the impurity's local density of states. This low-temperature effective SIAM, which we dub as *reentrant* SIAM, behaves as a *replica* of the high-temperature (bare) SIAM. The second-stage RG flow (obtained through NRG), whose FO fixed point emerges for $T \approx \Delta < T_{K1}$, takes over once the RG flows away from the unstable first-stage SC fixed point. The intuitive picture that emerges from our analysis is that the first Kondo state develops through impurity screening by semiconducting electrons, while the second Kondo state involves screening by metallic electrons, once the semiconducting electrons are out of reach to thermal excitations ($T < \Delta$) and only the metallic (low) spectral weight inside the gap is available for impurity screening. This switch implies that the first Kondo cloud is much smaller than the second since the NRG results show that, for all parameter ranges analyzed, $T_{K2} \ll T_{K1}$. Last, but not least, we analyze a hybrid system formed by a QI "sandwiched" between an armchair graphene nanoribbon (AGNR) and a scanning tunneling microscope (STM) tip (an AGNR + QI + STM system), with respective couplings set to reproduce the generic model described above. The energy gap (2Δ) in the AGNR can be externally tuned by an electric-field-induced Rashba spin-orbit interaction. We analyzed this system for realistic parameter values, using NRG, and concluded that the reentrant SIAM, with its associated second-stage Kondo, is worthy of experimental investigation.

DOI: 10.1103/PhysRevB.101.125115

I. INTRODUCTION

Understanding the low-temperature physics of a many-body interacting system is always a challenging task. Despite the simple form of the mutual interaction between pairs of its constituents, such a system, collectively, ofttimes behaves in an unexpected manner. Indeed, this aspect of nature has been insightfully discussed in a seminal paper by Anderson [1]. Within this context, the archetypal example, in condensed matter physics, is that of the ground state of the many-body Kondo problem [2,3].

The Kondo physics of a single magnetic impurity coupled to a metallic host is a well-understood problem [3], which can be experimentally studied in detail by coupling a quantum dot (QD) to a metallic contact [4], while its essential physical properties are captured by the well-known single impurity Anderson model (SIAM) [5]. A renormalization-group (RG) analysis of the SIAM [6] shows that the system crosses over three different fixed points as the temperature is lowered: (i) the unstable free orbital (FO) fixed point, in which the impurity is effectively decoupled from the conduction band, (ii) the also unstable local moment (LM) fixed point, where the impurity acquires a highly fluctuating magnetic moment, and (iii) the stable strong coupling (SC) fixed point, in which the magnetic moment of the impurity becomes fully screened by the conduction band electrons. The characteristic temperature below which the impurity moment is screened is the so-called Kondo temperature T_K. The SIAM, so to speak, provides a rich, although the simplest, description of the Kondo physics in QDs. The scenario presented above provides a generic picture of the physics of the SIAM, which remains qualitatively valid whenever the density of states of the conduction electrons exhibits no special features close to the Fermi level. Richer Kondo physics can be found if the conduction band exhibits structures such as a pseudogap or zero-energy peaks, like van Hove singularities. These features have been studied in great detail by several authors [7].

An interesting, but less studied, situation is the case in which the conduction band is that of a semiconductor, i.e.,

---

[*] Corresponding author: gbmartins@ufu.br

a spectra characterized by a finite gap Δ. The richness of the Kondo physics resulting from the interplay between T_K and Δ has been studied since almost three decades ago using a variety of numerical and analytical techniques, for instance: quantum Monte Carlo (QMC), by Takegahara *et al.* [8,9] and Saso [10], poor man's scaling (PMS), $1/N$ expansion, noncrossing approximation (NCA) and QMC, by Ogura and Saso [11], using Green's function, within equation-of-motion techniques, plus Hartree-Fock, by Cruz *et al.* [12], density matrix renormalization group (DMRG), by Yu and Guerrero [13], numerical renormalization group (NRG), by Takegahara *et al.* [8,9] and Chen and Jayaprakash [14], density matrix NRG (DM-NRG), by Moca and Roman [15], as well as perturbation theory and the local moment approach, by Galpin and Logan [16,17].

The earliest results pointed to the existence of a Kondo ground state (a SC fixed point) whenever $\Delta < \Delta_c$, where the critical gap Δ_c should fulfill the relation $\Delta_c \lesssim T_K$, being T_K defined as the Kondo temperature for $\Delta = 0$. However, NRG results [8,14,15] have indicated that a finite critical gap Δ_c only exists *away* from half-filling, while at half-filling any arbitrarily small gap (i.e., any $\Delta > 0$) results in the ground state becoming a doublet, i.e., switching from the standard Kondo-singlet SC fixed point (for $\Delta = 0$) to a doublet LM fixed point. This qualitative difference (half-filling vs away-from-half-filling) has been confirmed by analytical calculations [16] and the local moment approach [17], where it was shown that the ground state away from half-filling is a so-called generalized Fermi liquid, while it is a non-Fermi liquid for all finite values of Δ at half-filling. In addition, DM-NRG calculations [15] studied the quantum phase transition (QPT) occurring away from half-filling for $\Delta = \Delta_c$ and showed the formation of a single bound state when the system is in the SC regime ($\Delta < \Delta_c$), and the formation of an additional one once the system transitions to the LM regime ($\Delta > \Delta_c$).

In this work, we study two systems: the first is a slightly different model from the one already analyzed in the works described above, as it is composed of a QD [or a quantum impurity (QI)] that is *strongly* coupled on the right to a semiconducting lead (with a gap 2Δ) and on the left it is *weakly* coupled to a *metallic* lead (see Fig. 1). The second system, which we believe to be a feasible experimental realization of the model just described, is based on a QI strongly coupled to an armchair graphene nanoribbon (AGNR), which is in an externally induced insulating phase [18], and weakly coupled, through a small coupling Γ_{tip}, to a scanning tunneling microscope (STM) tip (modeled as a *metalliclike* band). This AGNR + QI + STM system is particularly attractive, as Kondo physics in carbon-based materials, mainly in *bulk* samples, has attracted a great deal of attention in the last few years [19–28]. The Kondo physics in graphene results from localized magnetic moments formed at vacancy sites [29–32] or through the surface deposition of magnetic atoms [33,34], in which the local density of states may be modified by either disorder [35,36] or by ripples induced by the underlying substrate [34]. Contrasting to the plethora of studies addressing the Kondo state in carbon nanotubes and on *bulk* graphene, less attention has been devoted to this effect in nanoribbon systems [37–40]. Depending on the shape of the edges of a graphene nanoribbon, either zigzag or armchair, its density of states near the Fermi level will be that of a semimetal, for zigzag nanoribbons, owing to the remarkable existence of metallic states localized at its edges, or it could alternate between being semiconducting or metallic, for armchair nanoribbons, depending on its width [41]. Interesting Kondo physics can be exploited from graphene nanoribbons, as recently shown by Li *et al.* [39], which reported an unexpected Kondo resonance behavior in a magnetic-molecule/Au(111) coupled system, in which an AGNR was used as a *bridge* to connect the molecule to the Au(111) surface, forming a hybrid structure. Their results showed that, thanks to their peculiar electronic properties, AGNRs were able to provide an effective coupling between the localized spin and the itinerant electrons in the Au(111) surface.

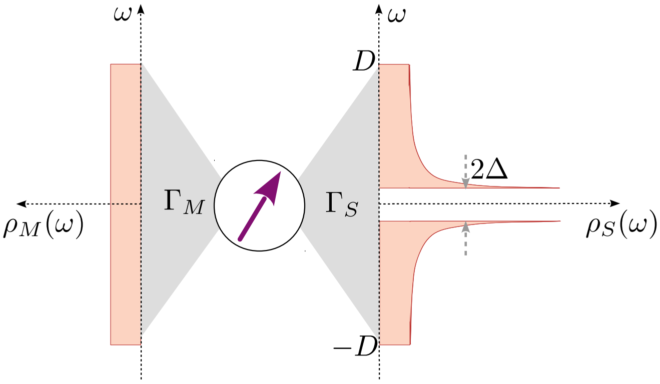

FIG. 1. Schematic representation of a QD coupled to a metallic lead (left) and to a semiconducting lead (right). The metallic lead is represented by a flat density of states $\rho_M(\omega)$, while the semiconducting lead is modeled by an energy-dependent density of states $\rho_S(\omega)$ characterized by a gap 2Δ. D is a cutoff energy and represents the bandwidth of conduction electrons and is taken as our energy unit.

The main result in this work is that the PMS and NRG analysis, of the appropriate SIAM for modeling the first system mentioned in the preceding paragraph, reveals, as one lowers the temperature, a sequence of *two* Kondo *stages*. Both are characterized by the traditional sequence of SIAM fixed points (FO-LM-SC), where the higher-temperature SC fixed point is unstable, with Kondo temperature T_{K1}, while the second stage has a stable SC fixed point with a much lower Kondo temperature T_{K2}. We dub the lower-temperature Kondo state as a "*reentrant* Kondo state," which is associated to an "emergent" effective SIAM, with an effective Hubbard U_{eff}, in contrast to the "bare" SIAM associated to the first-stage Kondo effect. The AGNR + QI + STM system, on the other hand, is a "real life" system where we claim, supported by NRG results for realistic parameters, the reentrant Kondo state may be experimentally observable.

The general organization of this work is as follows. In Sec. II we present the SIAM that describes the first system and the specific parameter values used. For the sake of completeness, in Sec. II A we disconnect the QI from the metallic band (keeping its coupling just to the semiconductor) and present a preliminary analysis, using Anderson's PMS [3,42], highlighting the interesting interplay between T_K and Δ. In Sec. II B, we additionally (weakly) couple the magnetic impurity to the metallic band and study, through an analysis of the impurity thermodynamic properties, as well as its local density of states (LDOS), an interesting effect, the *reentrant* Kondo effect, that can be briefly described as consisting of a sequence of two Kondo effects, where the Kondo temperature of the first (T_{K1}) is orders of magnitude higher that the second one (T_{K2}). Despite similarities with the so-called two-stage Kondo effect [43], there are important differences, the main one being that, in our system, the first Kondo effect is associated to an unstable SC fixed point, thus, there is only one true Kondo state, which occurs below T_{K2}. In Sec. III we apply the ideas developed for the reentrant Kondo effect to a real system, viz., a QI coupled to an AGNR and an STM tip (see Fig. 8). In Sec. IV we present a summary of the results, together with our conclusions.

II. MODEL AND NUMERICAL RESULTS

The first system that we have studied is schematically described in Fig. 1. In it, the semiconducting and the metallic density of states (DOS) seen by the QD are depicted to its right and left, respectively. As shown below, the presence of this metallic DOS will qualitatively change the many-body ground state of this system, in comparison to the ones analyzed in the literature, as described in the Introduction.

Thus, our model consists of an interacting QD coupled to a metallic lead, as well as to a semiconducting one (see Fig. 1). This system is modeled by a Hamiltonian $H_{\mathrm{SIAM}} = H_{\mathrm{imp}} + H_{\mathrm{S}} + H_{\mathrm{M}} + H_{\mathrm{Hyb}}$, whose first term is given by

$$H_{\mathrm{imp}} = \sum_{\sigma} \varepsilon_d d_\sigma^\dagger d_\sigma + U n_{d\uparrow} n_{d\downarrow}, \tag{1}$$

where $d_\sigma^\dagger$ (d_σ) creates (annihilates) an electron with energy ε_d and spin $\sigma = \uparrow\downarrow$ in the QD, $n_{d\sigma} = d_\sigma^\dagger d_\sigma$ is the QD occupancy, and U represents the Coulomb interaction. The leads are described by

$$H_{\mathrm{S/M}} = \sum_{\substack{\mathbf{k}\sigma \\ a=\mathrm{S,M}}} \varepsilon_{a\mathbf{k}} c_{a\mathbf{k}\sigma}^\dagger c_{a\mathbf{k}\sigma}, \tag{2}$$

where $c_{a\mathbf{k}\sigma}^\dagger$ ($c_{a\mathbf{k}\sigma}$) creates (annihilates) an electron with momentum $\mathbf{k}$, energy $\varepsilon_{a\mathbf{k}}$, and spin σ in the metallic ($a = \mathrm{M}$) or in the semiconducting ($a = \mathrm{S}$) lead. Finally, the QD-leads hybridization is given by

$$H_{\mathrm{Hyb}} = \sum_{\substack{\mathbf{k}\sigma \\ a=\mathrm{S,M}}} (V_{a\mathbf{k}} d_\sigma^\dagger c_{a\mathbf{k}\sigma} + \mathrm{H.c.}), \tag{3}$$

where $V_{a\mathbf{k}}$ represents the hybridization matrix element that couples the impurity either to the metallic ($a = \mathrm{M}$) or to the semiconducting ($a = \mathrm{S}$) lead. Here, we assume that the metallic lead is characterized by a flat DOS $\rho_M(\omega) = (1/2D)\Theta(D - |\omega|)$, where D is the half-bandwidth (Θ is the Heaviside step function), while the semiconducting-lead DOS (schematically shown in Fig. 1) is given by

$$\rho_S(\omega) = \rho_0 \frac{|\omega|}{\sqrt{\omega^2 - \Delta^2}} \Theta(|\omega| - \Delta)\Theta(D - |\omega|). \tag{4}$$

Here, 2Δ is the semiconducting gap and $\rho_0 = \frac{1}{2\sqrt{D^2-\Delta^2}}$ is a normalization factor. This particular expression for $\rho_S(\omega)$ [Eq. (4)] is appropriate for a dimerized chain, for instance, and was used in Ref. [12] to model the DOS of trans-polyacetylene. Its overall profile is schematically shown on the right side of Fig. 1, and it is very similar to the DOS of an AGNR [see Fig. 8(b)]. Assuming $V_{a\mathbf{k}} \equiv V_a$ to be $\mathbf{k}$ independent, for simplicity, the hybridization functions are defined as $\Gamma_a = \pi V_a^2 \rho_a$ (for $a = \mathrm{S,M}$).

The Kondo physics in our model, for $\Gamma_{\mathrm{S}} = 0$, corresponds to the traditional SIAM, which has been extensively studied over the last decades. In contrast, the situation where the QD couples solely to the semiconducting lead has received less attention (see the Introduction). Experimentally, the Kondo physics for magnetic impurities adsorbed in metallic surfaces has been studied through low-bias transport spectroscopy using an STM tip weakly coupled to the impurity. In our setup, the metallic lead serves not only to represent the STM tip, but also plays an important role in the NRG calculations, as it introduces a small, but finite, hybridization function at energies inside the semiconducting gap 2Δ (see Fig. 1).

In this work, we focus on the regime in which the QD is so weakly coupled to the metallic lead, in comparison to its coupling to the semiconducting lead ($\Gamma_{\mathrm{M}} \ll \Gamma_{\mathrm{S}}$), that any possible Kondo screening generated by conduction electrons in the metallic lead will occur at temperatures much lower than those associated to a possible Kondo screening occurring through electrons in the semiconducting lead. For our analysis in what follows, it is useful to define $\Gamma_0 = \Gamma_{\mathrm{M}} + \Gamma_{\mathrm{S}} \approx \Gamma_{\mathrm{S}}$.

Note that all the calculations presented in this work, aside from those in Sec. III, where different parameters (when considered) are explicitly stated, were done for the following parameter values: $D = 1$, the half-bandwidth, is our unit of energy, $U = 0.5$ is the Coulomb repulsion for impurity double occupancy, the impurity energy level is set at the particle-hole-symmetric point $\varepsilon_d = -U/2$, and $\Gamma_0 = 0.05$. The NRG approach was performed using Wilson's discretization parameter set to $\Lambda = 2.5$, 2000 many-body states were retained after each NRG iteration, and we made use of the z-trick averaging in the discretization procedure [44].

A. Interplay between T_K and Δ: Effective Kondo Hamiltonian and scaling analysis

To reveal the intricate interplay between T_K [45] and Δ, we will do a scaling analysis of the effective Kondo model, which can be derived from the SIAM by performing a Schrieffer-Wolff transformation [3,46]. For now, we are solely interested in the impurity plus semiconductor subsystem, thus, we set $V_{\mathrm{M}} = 0$. The resulting Kondo model can be written as

$$\begin{aligned} H_{\mathrm{K}} = {} & \sum_{\mathbf{k}\sigma} \varepsilon_{S\mathbf{k}\sigma} c_{S\mathbf{k}\sigma}^\dagger c_{S\mathbf{k}\sigma} + \sum_{\mathbf{k}\mathbf{k}'} J_{S\mathbf{k}\mathbf{k}'} [S^z (c_{S\mathbf{k}\uparrow}^\dagger c_{S\mathbf{k}'\uparrow} - c_{S\mathbf{k}\downarrow}^\dagger c_{S\mathbf{k}'\downarrow}) \\ & + S^+ c_{S\mathbf{k}\downarrow}^\dagger c_{S\mathbf{k}'\uparrow} + S^- c_{S\mathbf{k}\uparrow}^\dagger c_{S\mathbf{k}'\downarrow}], \end{aligned} \tag{5}$$

where $J_{S\mathbf{k}\mathbf{k}'}$ is a Kondo coupling that can be written in terms of the SIAM parameters. For simplicity, we assume $V_{S\mathbf{k}}$ to be $\mathbf{k}$ independent and real, thus denoting it by V_S, resulting in $J_{S\mathbf{k}\mathbf{k}'} \approx J_S = V_S^2(\frac{1}{U+\varepsilon_d} - \frac{1}{\varepsilon_d})$. (Note that, in what follows, for reasons that will be apparent soon, we will refer to J_S as the bare coupling and denote it as $J_S^{(0)}$.) In the above, we have neglected a scalar scattering potential, which in fact vanishes at the $\varepsilon_d = -U/2$ particle-hole-symmetric point. Following Anderson's original idea [3,42], the scaling analysis consists of integrating out the degrees of freedom in the conduction band whose energies lie within the interval $[D - \delta D, D]$, for electrons, and $[-D, -D + \delta D]$, for holes, where $\delta D > 0$. By doing so, we obtain an effective Kondo Hamiltonian where now the electrons are within a narrowed $\tilde{D} = D - \delta D$ conduction bandwidth, and with a renormalized coupling $\tilde{J}_S$, which obeys the scaling equation

$$\frac{d\tilde{J}_S}{d(\ln \tilde{D})} = -2\rho_S(\tilde{D})\tilde{J}_S^2. \tag{6}$$

This equation has to be integrated from D to some arbitrary energy $\tilde{D} < D$. Using Eq. (4) for ρ_S, we obtain the general solution

$$\frac{1}{\tilde{J}_S(\tilde{D})} - \frac{1}{\tilde{J}_S(D)} = 2\rho_0\left[\ln\left(\frac{\Delta}{D+\sqrt{D^2-\Delta^2}}\right)\Theta(\Delta - \tilde{D}) + \ln\left(\frac{\tilde{D}+\sqrt{\tilde{D}^2-\Delta^2}}{D+\sqrt{D^2-\Delta^2}}\right)\Theta(\tilde{D} - \Delta)\right], \tag{7}$$

where $\tilde{J}_S(D) = J_S^{(0)}$ is the initial condition, which corresponds to (as mentioned above) the so-called bare Kondo coupling (i.e., the coupling before the rescaling of the conduction band). As $\tilde{D}$ decreases, the expected SC fixed point is reached when $J_S(\tilde{D}) \to \infty$. At this fixed point, the impurity and the conduction electrons form a many-body Kondo singlet. Within the PMS, the value of D^*, defined as $\tilde{J}_S(\tilde{D} = D^*) = \infty$, is identified with the Kondo temperature of the system.

The two terms inside the square brackets on the right-hand side of Eq. (7), each multiplied to a different Heaviside step function, will thus be finite for different intervals of $\tilde{D}$: the first term for $\tilde{D} < \Delta$ and the second one for $\tilde{D} > \Delta$. This implies, as we shall see, a qualitative change in the solutions when $\tilde{D}$ crosses Δ. Starting with $\tilde{D} < \Delta$ (thus the second term vanishes), we obtain that

$$\frac{1}{\tilde{J}_S(\tilde{D})} - \frac{1}{J_S^{(0)}} = 2\rho_0 \ln\left(\frac{\Delta}{D+\sqrt{D^2-\Delta^2}}\right), \tag{8}$$

which results in a finite, but constant, coupling $\tilde{J}_S(\tilde{D})$, for any finite Δ. Hence, no strong coupling fixed point [i.e., no divergence of $\tilde{J}_S(\tilde{D})$] is expected.

On the other hand, the solution to Eq. (7) for $\tilde{D} > \Delta$ [first term in Eq. (7) vanishes], given by

$$\frac{1}{\tilde{J}_S(\tilde{D})} - \frac{1}{J_S^{(0)}} = 2\rho_0 \ln\left(\frac{\tilde{D}+\sqrt{\tilde{D}^2-\Delta^2}}{D+\sqrt{D^2-\Delta^2}}\right), \tag{9}$$

allows for an infinite $\tilde{J}_S(\tilde{D})$. Indeed, by setting $1/\tilde{J}_S(D^*) = 0$ in Eq. (9), after some algebraic manipulations we obtain that D^* can be written as

$$D^* = \frac{1}{2}\left[(D + \sqrt{D^2-\Delta^2})e^{-g} + \frac{\Delta^2}{D+\sqrt{D^2-\Delta^2}}e^{g}\right], \tag{10}$$

where $g = (2\rho_0 J_S^{(0)})^{-1}$. Obviously, D^* is meaningful only if it lies within the interval $\Delta < D^* < D$. Upon imposing this condition on Eq. (10), we find that, for a given Δ, the bare coupling $J_S^{(0)}$ has to be larger than a critical J_c, given by [47]

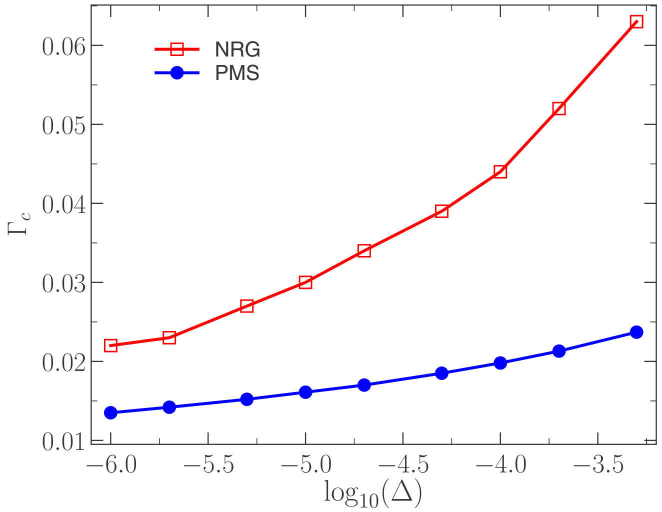

FIG. 2. Γ_c obtained by PMS [(blue) dots], Eq. (12), and by NRG [(red) squares], as a function of Δ (in log scale). The bare parameter values were $U = 0.5$ and $\varepsilon_d = -0.25$.

$$\rho_0 J_c = \frac{1}{2}\left[\ln\left(\frac{D+\sqrt{D^2-\Delta^2}}{\Delta}\right)\right]^{-1}. \tag{11}$$

As mentioned in the Introduction, we know that this is an artifact of the poor man's scaling approach since, at half-filling, as shown through NRG and confirmed by other methods, there is no SC fixed point for any finite gap Δ in the semiconductor spectra. In the following, we will compare the critical coupling given by Eq. (11) with the numerical results obtained from NRG calculations for the corresponding Anderson model. To do so, it is convenient to express J_c in terms of the Anderson model parameters. Defining $\Gamma_S^{(0)} = \pi V_S^2 \rho_0$, we can write $J_S^{(0)} = 4V_S^2/U = 4\Gamma_S^{(0)}/(\pi\rho_0 U)$, at the particle-hole-symmetric point [48]. Thus, Eq. (11) can be rewritten as

$$\Gamma_c = \frac{\pi U}{8}\left[\ln\left(\frac{D+\sqrt{D^2-\Delta^2}}{\Delta}\right)\right]^{-1}. \tag{12}$$

In Fig. 2, we plot Γ_c vs Δ (in log scale) for $U = 0.5$ and $\varepsilon_d = -0.25$, as obtained through the expression in Eq. (12) (blue dots) and compare it with the critical Γ_c obtained by NRG (red squares). To determine whether there is a tendency to Kondo screening or not in the NRG calculations, we monitor the impurity magnetic moment $\mu_{\text{imp}}^2(T) = k_B T \chi_{\text{imp}}(T)$ for decreasing temperature (not shown). Following Wilson's criterion [3], we say that the Kondo screening takes place only if $\mu_{\text{imp}}^2(T)$ becomes smaller than 0.07 as the system is cooled down. Thus, Γ_c is defined as the smallest value of Γ, as obtained through NRG (red squares in Fig. 2), for which this condition is still satisfied. It is interesting to notice that the Γ_c obtained by NRG is systematically larger than the one obtained by PMS [Eq. (12)]. We note that there is a qualitative agreement between the PMS and NRG results, showing that Γ_c increases with Δ. This means that, as intuitively expected, a larger Δ requires stronger hybridization between the

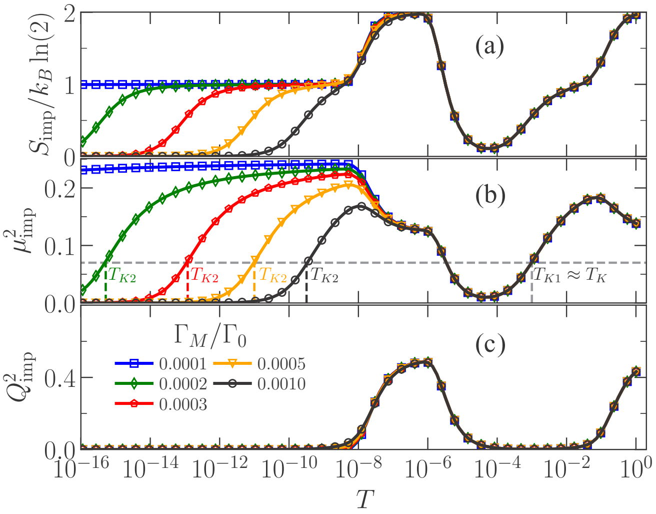

FIG. 3. Impurity contribution to (a) entropy S_{imp}, (b) magnetic moment μ^2_{imp}, and (c) charge fluctuation Q^2_{imp}, as a function of temperature for $10^{-4} < {}^{\Gamma_{\mathrm{M}}}/_{\Gamma_0} < 10^{-3}$ and $\Delta = 10^{-5}$. Note the appearance of a second SC fixed point (for all ${}^{\Gamma_{\mathrm{M}}}/_{\Gamma_0} \geqslant 0.0002$) at lower temperatures, which can be identified by an increase in charge fluctuation at around $T \approx 10^{-5}$ [(c)], followed by an LM regime, followed by an impurity-band singlet formation [(b)] at the second SC fixed point, with lowering onset temperature, as Γ_{M} decreases. To facilitate the discussion, the estimated values for T_{K1} and T_{K2} (obtained through Wilson's criterion) are indicated in (b). See text for details.

impurity and the (semiconducting) conduction electrons for the Kondo screening to take place. Last, but not least, taking into account that, as shown above, there is no SC fixed point for $\tilde{D} < \Delta$, the NRG results in Fig. 2 (red squares) do not describe the ground state of the $V_M = 0$ Hamiltonian, but rather what we may call a finite-temperature Kondo phase (see below) associated to an unstable SC fixed point. As described in the Introduction, the ground state of the $V_M = 0$ Hamiltonian corresponds to a doublet LM fixed point [16,17].

B. Reentrant effective Anderson Hamiltonian

Let us now turn our attention to the full system, which includes the metallic contact. In particular, we are interested in studying what happens to the system for temperatures below T_K, where, again, T_K is the Kondo temperature for $\Delta = 0$ and $V_M = 0$. To do this, we fix $\Gamma_0 = 0.05$ and $\Delta = 10^{-5}$, and vary Γ_{M}. Note that, as can be checked from the NRG curve in Fig. 2 (red squares), for these parameter values we have that $\Gamma_0 > \Gamma_c$. Our results now rely just on NRG calculations since PMS breaks down before $\tilde{D} < \Delta$, as shown in the previous section. We will see that an intriguing "revival" of an effective Anderson Hamiltonian is observed as the temperature tends to zero. This assertion will become clear after we analyze the impurity thermodynamic properties, where it will become evident the appearance of the two Kondo temperatures mentioned in Sec. I, T_{K1} and T_{K2}, with $T_{K1} \gg T_{K2}$ [see Fig. 3(b)]. In addition, it should be noted that, as expected [and indicated in Fig. 3(b)], the higher Kondo temperature T_{K1}, obtained for finite Γ_M and Δ, has approximately the same value as the Kondo temperature T_K, corresponding to the $\Gamma_M = \Delta = 0$ case, as long as Γ_M and Δ are $\ll T_K$.

Figure 3 shows the impurity contribution to the entropy S_{imp} [Fig. 3(a)], magnetic moment μ^2_{imp} [Fig. 3(b)], as well as the charge fluctuations Q^2_{imp} [Fig. 3(c)], as a function of temperature for five different values of Γ_{M} in the interval $10^{-4} \leqslant {}^{\Gamma_{\mathrm{M}}}/_{\Gamma_0} \leqslant 10^{-3}$. We first note that, for temperatures in the interval $10^0 > T \gtrsim 10^{-5} = \Delta$, all impurity thermodynamic properties are independent of Γ_{M}, and the results display the traditional SIAM behavior, in which the system crosses over from the FO to the LM to an SC fixed point, as the temperature decreases. These three fixed points are marked, respectively, by entropy values ${}^{S_{\mathrm{imp}}}/_{k_B} \sim \ln 4$, $\sim \ln 2$, and ~ 0, as seen in Fig. 3(a). This is accompanied by an enhancement of the magnetic moment μ^2_{imp}, at the LM fixed point, followed by its complete suppression in the SC fixed point, as shown in Fig. 3(b). Finally, notice also the strong suppression of the impurity charge fluctuations Q^2_{imp} (at the LM and SC points) [Fig. 3(c)]. Interestingly, as mentioned above, all these features are independent of the Γ_{M} value. This can be easily concluded from the superposition of all the curves in all panels in Fig. 3 in the temperature interval $10^0 > T \gtrsim 10^{-5}$. This behavior may be associated to the fact that the largest Γ_{M} used in the results shown in Fig. 3 (given by $10^{-3}\Gamma_0 = 5 \times 10^{-5}$) was still much smaller than $T_K \approx 10^{-3}$.

It is well known that the thermodynamic properties presented above (for the temperature interval $10^0 > T \gtrsim 10^{-5}$) are characteristic of the SIAM [3]. However, for a *traditional* SIAM, the values of the thermodynamic quantities, for $T \ll T_K$, i.e., well into the SC regime, remain unchanged down to $T \to 0$, as the system would have already reached the stable SC fixed point and would stay there. Remarkably, in the present case, when T approaches $\Delta = 10^{-5}$ (from above), the system deviates from this standard behavior, as it can be easily seen in Fig. 3, since all thermodynamic properties have additional structures for $T < \Delta$. Indeed, when $T \to \Delta$, the system flows to a *second* free orbital (SFO) fixed point, marked by an increase of S_{imp}, μ^2_{imp}, and Q^2_{imp}, to values that go back to their high-temperature ($T = D$) values. Further decrease of T shows that the system crosses over fixed points that have very similar properties to the ones crossed in the temperature interval $10^0 > T \gtrsim 10^{-5}$. The similarity between the low- and high-temperature fixed points indicates that, for $T < \Delta$, the system seems to be governed by an *effective* SIAM with renormalized parameters and a much lower Kondo temperature. Note that the extent of the plateaus in the entropy (at $k_B \ln 2$) and in the magnetic moment (at $\approx \frac{1}{4}$), which mark how long the system stays close to the LM fixed point, depend strongly on Γ_{M}, showing that the Kondo temperature for the reentrant effective SIAM, denoted as T_{K2}, depends strongly on Γ_{M}. To highlight that, in Fig. 3(b) we use Wilson's criterion to determine the characteristic Kondo temperatures T_{K1} and T_{K2}, which can be extracted from the intersection of the gray dashed line (corresponding to $\mu^2_{\mathrm{imp}} = 0.07$) with the μ^2_{imp} curves for different Γ_{M} values. The higher Kondo temperature, T_{K1}, indicated on the right side of Fig. 3(b), which is clearly independent of Γ_{M}, and similar to the $\Delta = \Gamma_{\mathrm{M}} = 0$ Kondo temperature T_K, is accompanied by a Γ_{M}-dependent T_{K2} Kondo temperature, much lower than T_{K1} and associated

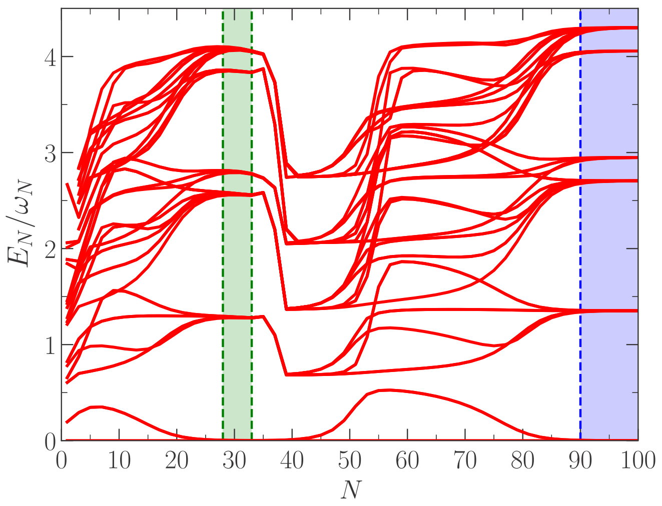

FIG. 4. Energy spectrum vs NRG iteration step N (odd values only) obtained for the lowest-energy levels. Note the fixed points in the traditional Anderson model seen in the iterations ranging from $N \approx 5$ to $N \approx 35$, which are traversed again at higher N values ($N \gtrsim 41$), showing the reentrance of the Anderson model behavior at low energies. The model parameters used here were $\Gamma_0 = 0.05$, $\Gamma_\text{M}/\Gamma_0 = 5 \times 10^{-4}$.

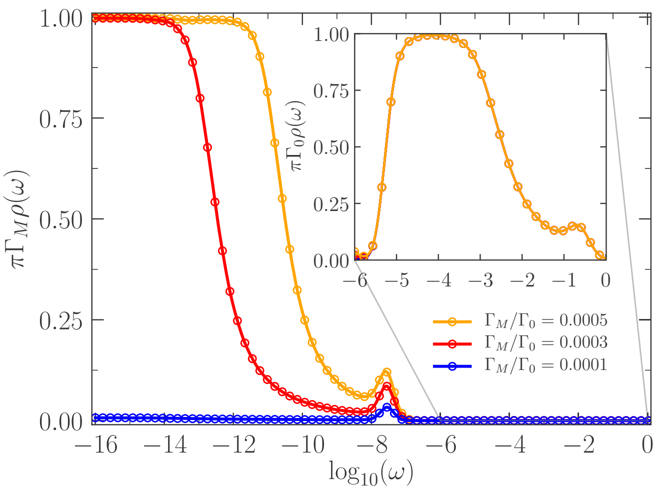

FIG. 5. Impurity LDOS as a function of energy for $\Gamma_0 = 0.05$ and three values of Γ_M. The inset shows a zoom-in of the region where the first Kondo regime occurs. The LDOS $\rho(\omega)$, in the main panel and in the inset, is multiplied by $\pi\Gamma_\text{M}$ and $\pi\Gamma_0$, respectively, so as to show that both Kondo regimes obey the Friedel sum rule.

to a stable SC fixed point. Thus, the thermodynamic quantities (S_imp, μ^2_imp, and Q^2_imp) exhibit a behavior compatible with an NRG flow through a low-temperature *second-stage* effective SIAM, as will be explicitly shown next.

Indeed, this interesting (and unusual) behavior can be clearly captured by the energy flow diagram obtained from NRG, as shown in Fig. 4, which displays the energy spectrum as function of the NRG iteration step N (for odd values). As described in Ref. [6], the occurrence of a fixed point in the iterative NRG procedure can be determined by looking for a set of many-particle energy levels that repeat themselves in a sequence of odd (or even) steps in the NRG diagonalization procedure. Figure 4 shows that the traditional SIAM fixed points are observed in the range of iterations from $N \approx 5$ to $N \approx 35$, while the second-stage SIAM fixed points are traversed again at higher N values ($N \gtrsim 41$). For the sake of clarity, we added a green-shaded vertical stripe to highlight the (unstable) SC fixed point and a blue-shaded one to highlight the second (stable) SC fixed point. The parameters used were $\Gamma_0 = 0.05$, $\Gamma_\text{M}/\Gamma_0 = 5 \times 10^{-4}$, the same as for the inverted triangle curves in Fig. 3.

Further insight onto the two SC fixed points can be gained from the analysis of the impurity's LDOS, given by

$$\rho(\omega) = -\frac{1}{\pi}\text{Im}[\langle\langle d_\sigma; d_\sigma^\dagger\rangle\rangle_\omega], \tag{13}$$

where $\langle\langle d_\sigma; d_\sigma^\dagger\rangle\rangle_\omega$ is the retarded local Green's function in the energy domain, within Zubarev's notation [49]. We first analyze the impurity LDOS at low energies ($\omega < 10^{-7}$) in the main panel of Fig. 5, which shows $\pi\Gamma_\text{M}\rho(\omega)$ as a function of $\log_{10}\omega$ for three values of Γ_M. For $\Gamma_\text{M} = 3 \times 10^{-4}\,\Gamma_0$ and $\Gamma_\text{M} = 5 \times 10^{-4}\,\Gamma_0$ (red and orange curves, respectively), we see Kondo peaks that nicely obey the Friedel sum rule. Notice that, to accomplish this, we are multiplying $\rho(\omega)$ by $\pi\Gamma_\text{M}$, the impurity coupling to the metallic lead. This shows that the reentrant Kondo state, as expected, involves electrons from the metallic DOS. However, contrary to what happens for the two larger values of Γ_M, for $\Gamma_\text{M} = 10^{-4}\,\Gamma_0$ (blue curve), there is no Kondo peak at low energies (at least down to $\omega = 10^{-16}$). This is in agreement with the thermodynamic properties for the corresponding (blue) curves in Fig. 3, which show no indication of the occurrence of a reentrant Kondo effect. In addition, the widths of the two Kondo peaks in the main panel of Fig. 5, for $\Gamma_\text{M} = 3 \times 10^{-4}\,\Gamma_0$ and $\Gamma_\text{M} = 5 \times 10^{-4}\,\Gamma_0$, are in accordance with the estimated values for T_K using Wilson's criterion in Fig. 3(b). Finally, it is interesting to notice that the small peaks observed slightly above $\omega = 3 \times 10^{-8}$ correspond to the upper Hubbard peak, which is located at $\frac{U_\text{eff}}{2}$, where the renormalized Coulomb repulsion U_eff is associated to the effective reentrant SIAM (see more details below).

We now proceed to an analysis of the LDOS at higher values of ω. The inset in Fig. 5 shows a zoom of the $\omega \in [10^{-6}, 1]$ energy window. Note that, in accordance with the thermodynamic quantities analyzed in Fig. 3, all three curves collapse onto each other. In addition, as was the case at lower energies (main panel), if one multiplies $\rho(\omega)$ by $\pi\Gamma_0$ (as done in the inset), the results obey the Friedel sum rule, indicating that, for the first SC fixed point, the many-body state is formed between the impurity and the electrons from the semiconducting DOS. The interpretation here is immediate: the higher peak corresponds to the first (T_{K1}) Kondo effect, while the smaller peak above $\omega = 10^{-1}$ corresponds to the upper Hubbard peak, located at $\frac{U}{2}$.

The LDOS results just presented in Fig. 5 provided access to the numerical value of U_eff (the small peak in the main panel). Since it, together with Γ_S, Γ_M, and U, characterizes the thermodynamic properties shown in Fig. 3, we will, in what follows, correlate (and summarize) the results presented in Fig. 3 with those presented in Fig. 5. In Fig. 3, one can clearly see that, as the temperature decreases below the first Kondo temperature $T_{K1} \approx 10^{-3}$, the system enters the SFO fixed point (for $T \approx \Delta = 10^{-5}$), where the coupling between

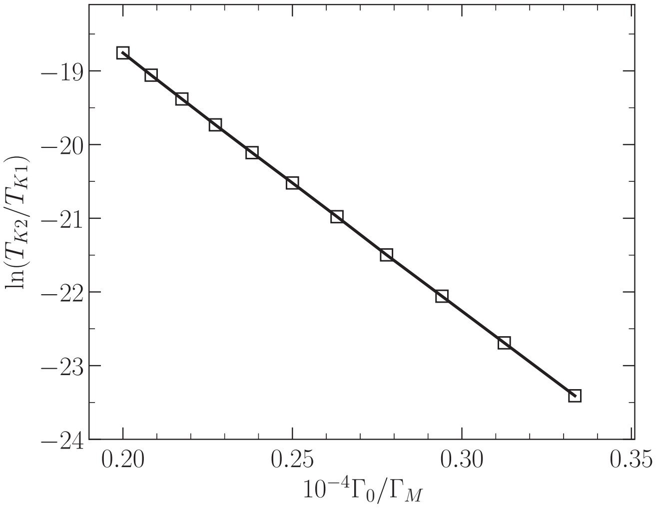

FIG. 6. $\ln(T_{K2}/T_{K1})$ vs $10^{-4} \times \Gamma_0/\Gamma_{\rm M}$, for $\Gamma_0 = 0.05$. From the linear behavior of the curve, the data could be fitted to an expression like $T_{K2} = A_0 e^{-A_1/\Gamma_{\rm M}}$.

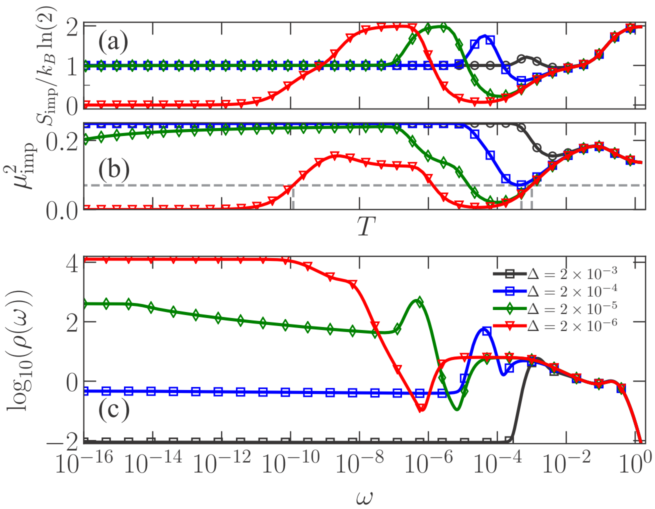

FIG. 7. (a) Impurity entropy $S_{\rm imp}$ and (b) magnetic moment $\mu^2_{\rm imp}$, as a function of T, and (c) $\log_{10}[\rho(\omega)]$ vs energy, for $\Gamma_0 = 0.05$, $\Gamma_{\rm M} = 5 \times 10^{-4}$, and four Δ values ($2.0 \times 10^{-6} \leqslant \Delta \leqslant 2 \times 10^{-3}$). The horizontal gray dashed line in (b) represents $\mu^2_{\rm imp} = 0.07$, and from its intersection with the $\mu^2_{\rm imp}$ curves we obtain T_{K1} and T_{K2} for each Δ value. In (c), we have chosen to show $\log_{10}[\rho(\omega)]$ to visualize all the peaks, as their heights differ by several orders of magnitude. Note that the horizontal axis scale (not shown) in (a) and (b) is the same as in (c).

the impurity and the conduction electrons drops from Γ_0 to $\Gamma_{\rm M}$, in which case we have that $T \gtrsim \Gamma_{\rm M}$, and $T \gg U_{\rm eff} \approx 3 \times 10^{-8}$ (see Fig. 5). As the temperature decreases further, the system then enters the second LM fixed point for $T \lesssim U_{\rm eff} \approx 3 \times 10^{-8}$ (compare Figs. 3 and 5). Finally, when T goes below the second Kondo temperature [T_{K2}, whose value depends strongly on $\Gamma_{\rm M}$, see Figs. 3(b) and main panel of 5] the system reaches the stable SC fixed point.

The existence of this very small $U_{\rm eff}$ can be inferred from the PMS analysis of the Anderson model, as discussed by Jefferson [50] and Haldane [51] for metallic conduction bands, and, later on, extended to more general spectra in Refs. [52,53] [see, for instance, Eq. (27) of Ref. [53]]. Although these analyses are limited by their perturbative character, they suggest that the renormalized Coulomb repulsion indeed decreases along the RG flow.

Since the width of the Kondo peak at half-height is a good estimate of the Kondo temperature, calculations for various values of $\Gamma_{\rm M}$, at fixed Γ_0, like the ones done in Fig. 5, provide the dependence of the Kondo temperature of the reentrant Kondo screening T_{K2} on $\Gamma_{\rm M}$. These results are shown in Fig. 6, where we plot $\log(T_{K2}/T_{K1})$ as a function of $\Gamma_0/\Gamma_{\rm M}$ (for $\Gamma_0 = 0.05$, in units of 10^{-4}). The remarkable linear behavior of the curve suggests a fitting of the NRG results to an expression like $T_{K2} = A_0 e^{-A_1/\Gamma_{\rm M}}$, where both A_0 and A_1 are positive and $A_0 \propto T_{K1}$. This expression indicates that T_{K2} decreases exponentially with a decreasing $\Gamma_{\rm M}$. The parameters A_0 and A_1 contain the intricate information about the reentrant effective SIAM.

Before closing this section, in Fig. 7 we show how both Kondo screenings change, in respect to the gap Δ in the semiconducting lead. Figures 7(a)–7(c) show the impurity entropy $S_{\rm imp}$, magnetic moment $\mu^2_{\rm imp}$, and LDOS $\rho(\omega)$, respectively, for four different Δ values ($2.0 \times 10^{-6} \leqslant \Delta \leqslant 2 \times 10^{-3}$). The calculations were done for $\Gamma_0 = 0.05$ and $\Gamma_{\rm M} = 5 \times 10^{-4}$, which is an order of magnitude above the largest $\Gamma_{\rm M}$ value used in Fig. 3. Notice that, in Fig. 7(b) (as done also in Fig. 3), the characteristic Kondo temperatures T_{K1} and T_{K2}, for each value of Δ, can be extracted from the intersection of the gray dashed line (corresponding to $\mu^2_{\rm imp} = 0.07$) with the $\mu^2_{\rm imp}$ curves. It is straightforward to note that, for the smallest value of Δ analyzed [$\Delta = 2.0 \times 10^{-6}$ (red curve)], $S_{\rm imp}$ and $\mu^2_{\rm imp}$ are strongly suppressed in the temperature interval $10^{-5} \lesssim T \lesssim 10^{-4}$ and vanish as $T \to 0$ (below $T \approx 10^{-11}$), clearly showing the existence of two Kondo screening regimes, the first with $T_{K1} \approx 10^{-3}$ and the second with $T_{K2} \approx 10^{-10}$ [as indicated in Fig. 7(b)]. The impurity LDOS [Fig. 7(c)] for the same value of $\Delta = 2.0 \times 10^{-6}$ (red curve) exhibits, accordingly, two (not normalized) Kondo peaks, with respective heights $\frac{1}{\pi\Gamma_0}$ and $\frac{1}{\pi\Gamma_{\rm M}}$, for the first and second Kondo regimes, respectively. However, for the larger Δ values shown in Fig. 7, we note that the first Kondo regime is progressively suppressed. This occurs because, as Δ increases, Γ_c also increases, eventually becoming larger than 0.05, the Γ_0 value used in the calculations [see NRG results (red squares) in Fig. 2]. Figure 7(a) shows the details of how this behavior evolves. First, it is important to remark that, as shown in Fig. 3, the end of the first Kondo screening occurs for $T \approx \Delta$. Second, as can be seen in Figs. 7(a) and 7(b), the temperature at which the transition from the LM to the SC fixed point starts, for the first Kondo stage, does not depend on Δ. Thus, as Δ increases, the flow from LM to SC is cut short and the $T \to 0$ physics is that of the first LM fixed point (i.e., $S_{\rm imp} = k_B \ln 2$ and $\mu^2_{\rm imp} = \frac{1}{4}$). In other words, the first SC fixed point is squeezed out of existence by the increase in Δ and the system gets stuck in the first LM fixed point. The two $\Delta = 2.0 \times 10^{-6}$ Kondo peaks shown in the LDOS [Fig. 7(c), red curve], in turn, are progressively suppressed as

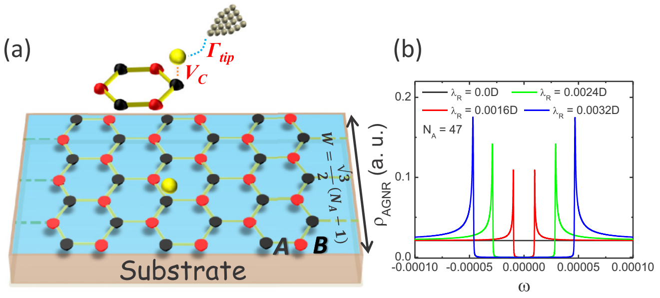

FIG. 8. (a) Schematic representation of an N_A-AGNR deposited on a substrate, with a magnetic impurity (yellow) deposited in a top-site configuration [right above a nanoribbon carbon atom (black), and strongly coupled to it, with hopping amplitude V_C]. Right on top of the magnetic impurity adatom (as shown in the inset) is located a weakly coupled *metallic* STM tip, with a coupling strength Γ_{tip}. (b) DOS for a 47-AGNR close to the Fermi level, without the impurity, as a function of energy ω, for different RSOI strengths λ_R. W is the width of the AGNR (assuming a nearest-neighbor distance $a_{C-C} = 1$), which depends on the number of dimmers N_A across the nanoribbon. Note that, as $N_A = 47 = 3 \times 16 - 1$, the $\lambda_R = 0.0$ DOS (black curve) is metallic, while a finite λ_R opens a gap in the spectra.

Δ increases [see the green, blue, and black curves in Fig. 7(c)], confirming the destruction of both Kondo screening regimes. Thus, the first LM fixed point becomes the low-temperature stable fixed point.

Finally, we have also checked how the impurity thermodynamic properties evolve when we vary Γ_{M} in the interval $10^{-6}\Gamma_0 < \Gamma_{\text{M}} < \Gamma_0$, while Γ_{S} takes values determined by $\Gamma_{\text{M}} + \Gamma_{\text{S}} = \Gamma_0$. The results (not shown), as Γ_{M} approaches Γ_0, show the gradual disappearance of all traces of the second Kondo stage, resulting in the usual impurity thermodynamic properties, traditional of a Kondo effect in a metallic host, with $T_K = T_{K1}$.

The results shown so far are quite general and may be applicable to a variety of gapped systems to which a magnetic impurity can be coupled. Examples encompass narrow-gap semiconductors [54], synthesized polymers [55], as well as modern gap-engineered materials [56]. In the following, we shall discuss how the reentrant SIAM behavior emerges in an AGNR in which a Rashba spin-orbit coupling (and thus a gap) is induced externally [57].

III. REENTRANT KONDO EFFECT IN ARMCHAIR GRAPHENE NANORIBBON

In this section, we discuss a plausible experimental setup consisting of a magnetic impurity coupled to an AGNR, subjected to a tunable spin-orbit coupling, in which the phenomena presented in Sec. II B may be experimentally observed.

It has been shown recently by Lenz *et al.* [57] that, under the influence of Rashba spin-orbit interaction (RSOI), due to an external electric field, or induced by a substrate, AGNRs exhibit a tunable band gap at the Fermi level [58]. In the following, we will consider a magnetic impurity coupled to such a gapped AGNR and weakly coupled to an STM tip (see Fig. 8). By employing a tight-binding model, combined with NRG calculations, we show that this setup is very convenient to investigate the reentrant Kondo effect discussed in Sec. II B.

It is important to notice that, as already mentioned above, an AGNR may be metallic (when the number of dimers N_A across its width W is such that $N_A = 3M + 1$, where M is an integer), or semiconducting (for other values of N_A). The use of an *intrinsic* semiconducting AGNR for the purpose of testing the reentrant Kondo effect would be problematic for two reasons: first, the typical gap values Δ that one obtains are in general *large* and, second, they are hard to tune. The proposal of using RSOI to produce a small and tunable gap Δ in a metallic AGNR, as illustrated in Fig. 8(b), sidesteps both problems at once.

Our proposed setup is schematically shown in Fig. 8(a). The system, comprised of a single magnetic impurity coupled to an AGNR, is modeled by the standard SIAM-like Hamiltonian [5], given by

$$H = H_{\text{AGNR}} + H_{\text{imp}} + H_{\text{tip}} + H_{\text{AGNR-imp}} + H_{\text{imp-tip}}, \tag{14}$$

where the first term describes the AGNR, which is modeled by a tight-binding Hamiltonian in real space, given by

$$H_{\text{AGNR}} = \sum_{i\sigma}(\varepsilon_0 - \mu)c^\dagger_{i\sigma}c_{i\sigma} + \sum_{\langle i,j\rangle,\sigma\sigma'}[t_{ij}\delta_{\sigma\sigma'} + i\lambda_R\hat{\mathbf{z}}\cdot(\mathbf{s}\times\boldsymbol{\delta}_{ij})]c^\dagger_{i\sigma}c_{j\sigma'}, \tag{15}$$

where $c^\dagger_{i\sigma}$ ($c_{i\sigma}$) creates (annihilates) an electron with energy ε_0 and spin σ on the ith site of the AGNR, and μ is the chemical potential, which can be externally tuned by a back gate. The second term is the nearest-neighbor π-band tight-binding Hamiltonian, where $t_{ij} = t_0$ is the hopping between nearest-neighbor sites [59], with $t_0 \approx 2.7$ eV [60]. The third term models the induced RSOI, with parameter λ_R proportional to the electric field applied perpendicular to the x-y plane of the nanoribbon [61,62], $\mathbf{s} = (s_x, s_y, s_z)$ represents a vector of Pauli spin matrices, and $\boldsymbol{\delta}_{ij}$ are the vectors connecting nearest-neighbor sites. The second term of Eq. (14) describes the single-level Anderson impurity [given by Eq. (1), in Sec. II], while the third term describes the STM tip, which is modeled by the Hamiltonian H_{M} in Eq. (2). The fourth term in Eq. (14), which couples the impurity to the AGNR, is given by

$$H_{\text{AGNR-imp}} = \sum_{j,\sigma} V_{j\sigma}(c^\dagger_{j\sigma}d_\sigma + \text{H.c.}), \tag{16}$$

where the most general situation is that in which the index j runs over a number of sites in the AGNR that are closest to the impurity. In Fig. 8(a), we depict the situation where the impurity couples to just one site. Finally, the last term in Eq. (14), which couples the impurity to the STM tip, reads as

$$H_{\text{imp-tip}} = \sum_{\mathbf{k}\sigma}(V_{\mathbf{k}}c^\dagger_{\mathbf{k}\sigma}d_\sigma + \text{H.c.}). \tag{17}$$

In Eq. (16), if we consider the situation depicted in Fig. 8, where the impurity couples to a single carbon atom in the ribbon, then, assuming that the RSOI has no effect over this coupling (thus, the coupling is spin independent), we can set $V_{j\sigma} \equiv V_C$. Furthermore, assuming a constant density of states at the metallic tip ρ_{tip}, we may write the tip-impurity hybridization function as $\Gamma_{\text{tip}} = \pi V^2_{\text{tip}}\rho_{\text{tip}}$, where V_{tip} is the hopping parameter between the impurity and the STM tip. Thus, $\Gamma_{\rm tip} \equiv \Gamma_{\rm M}$, as defined in Sec. II. Therefore, from now on, to facilitate the comparison with the results in Sec. II, we will denote the QI-STM coupling by $\Gamma_{\rm M}$ (instead of $\Gamma_{\rm tip}$) to present all the forthcoming results.

To perform the NRG calculations to tackle the Kondo effect in this system, we need to calculate the hybridization function $\Gamma_0(\omega)$ [6,7]. To do that, we have implemented a recursive Green's function approach [63,64] for the noninteracting case, i.e., $U = 0$. Having the local Green's function at hand [40], we can obtain the self-energy matrix for the impurity, $[\mathbf{\Gamma}_{\rm AGNR+tip}]_{\sigma\sigma'}(\omega) = {\rm Im}[\mathbf{G}^{-1}_{\rm C+tip}(\omega)]_{\sigma\sigma'}$, where $\mathbf{G}_{\rm C+tip}$ is the AGNR + tip [65] noninteracting, local (at the impurity site), Green's function matrix. We assume the magnetic impurity placed at a top-site configuration [66], as depicted in Fig. 8, in which case the system is still bipartite and the particle-hole symmetry of the whole system is preserved [67]. This is important, as it allows for a direct comparison of the results in this section with those in Sec. II. Finally, note that, as the RSOI does not break time-reversal symmetry, we have that the $\mathbf{\Gamma}_{\rm AGNR+tip}$ matrix is diagonal, thus, $[\mathbf{\Gamma}_{\rm AGNR+tip}]_{\uparrow\uparrow} = [\mathbf{\Gamma}_{\rm AGNR+tip}]_{\downarrow\downarrow} \equiv \Gamma_0$ [65].

For concreteness, we consider a metallic AGNR, of width $W = \sqrt{3}(N_A - 1)/2$, where N_A is the number of dimmers along the transverse direction [see Fig. 8(a) for details]. Moreover, we have chosen the carbon-carbon hopping amplitude $t \approx 1/3.1$, so that the half-bandwidth is $D = 1$, thus consistent with Sec. II, where the half-bandwidth was taken as the energy unit. Figure 8(b) shows the DOS $\rho_{\rm AGNR}(\omega)$ for a 47-AGNR, close to the Fermi level, for a pristine nanoribbon, i.e., without any impurity coupled to its surface, for different values of RSOI. We clearly see that in the absence of RSOI ($\lambda_R = 0$) our AGNR exhibits a gapless DOS as shown by the black line in Fig. 8(b). However, a finite λ_R induces a gap Δ around the Fermi level as shown by the red ($\lambda_R = 1.6 \times 10^{-3}$), green ($\lambda_R = 2.4 \times 10^{-3}$), and blue ($\lambda_R = 3.2 \times 10^{-3}$) curves in Fig. 8(b), for progressively larger values of λ_R. Thus, the AGNR with finite RSOI simulates the semiconducting band coupled to the impurity, while the STM tip plays the role of the metallic band defined in Sec. II, introducing a small but finite broadening of the impurity level $\Gamma_{\rm M}$ inside the gap. It is worthwhile to remark that (i) the RSOI-induced gap Δ has a particular dependence for narrow AGNRs as a function of λ_R, especially for large values of λ_R [57]. However, Δ decreases as the width of a metallic AGNR increases, such that, in the limit where border effects over the electronic structure vanish, the spin degeneracy will be lifted, but with no band gap, as expected for *bulk* graphene [61,68]; (ii) Δ exhibits a small oscillation as a function of λ_R [57]. In our calculations, we restrict λ_R to a range within which Δ increases monotonically with λ_R (for a fixed width), and, importantly, in agreement with experimental RSOI values in graphene [69–71].

In what follows, we set $\Gamma_{\rm M} = 1.0 \times 10^{-6}$ (thus, fixing $V_{\rm tip}$), $V_C = 0.258$, and $N_A = 47$ (corresponding to $W \approx 5.65$ nm). Differently from the case of a zigzag graphene nanoribbon, where the hybridization function is strongly dependent on what site (across the ribbon) one chooses to couple the impurity to [40] (i.e., close or away from the nanoribbon's edge), for an AGNR we have noticed a small quantitative difference, as the $\rho_{\rm AGNR}(\omega)$ along the width has a small variation. Therefore, we considered the impurity position fixed at a given top-site location [66] for all the following calculations. The resulting hybridization function $\Gamma_0(\omega)$, for various values of λ_R, is shown in Fig. 9. To make the region near the Fermi level (located slightly to the left of the left axis) more visible, we plot the energy axis in logarithm scale, restricted to $\omega > 0$ [by virtue of particle-hole symmetry, we have that $\Gamma_0(-\omega) = \Gamma_0(\omega)$]. As expected, for $\lambda_R = 0.0$ the AGNR is metallic, therefore, $\Gamma_0(\omega)$ has a constant value (≈ 0.01) around the Fermi level. In this case, our system behaves quite similarly to a QI coupled to a metallic DOS with a flat band. However, for finite λ_R we clearly see the formation of a small gap Δ, which increases with λ_R. In the inset of Fig. 9 we show how $\Gamma_0(0)$ evolves with λ_R. We note that $\Gamma_0(0)$ has a small residual and finite value inside the RSOI induced gap, originating from the *localized* impurity state contribution, which decreases as λ_R (or Δ) increases, eventually saturating at $\Gamma_0(0) \approx \Gamma_{\rm M} = 1.0 \times 10^{-6}$. This behavior results from a mixing of spin channels in the conduction band mediated by the RSOI, reducing the spin-preserving transmission at the Fermi level, as when RSOI is switched on the spin-flip mechanism is allowed in the AGNR. This band-gap-induced RSOI will show its fingerprints in the impurity thermodynamic properties, determining the reentrant SIAM behavior.

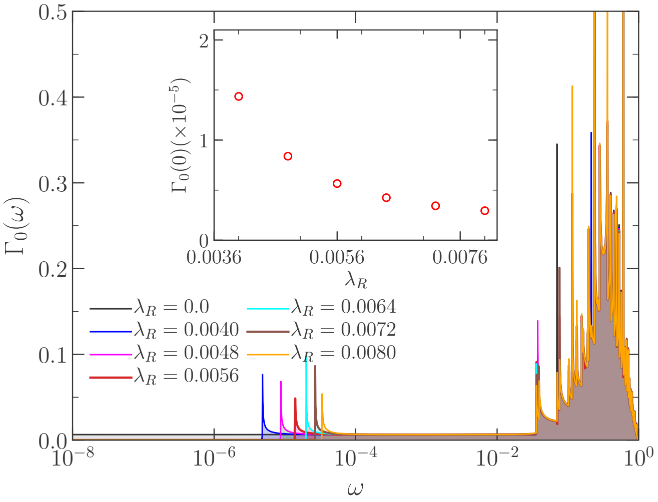

FIG. 9. Hybridization function $\Gamma_0(\omega)$ for vanishing λ_R (black curve) and in the interval $0.004 \leqslant \lambda_R \leqslant 0.008$. The range of values of λ_R was chosen in order to produce Δ values monotonically increasing with λ_R. The inset shows $\Gamma_0(0)$ as a function of λ_R. Parameter values are $V_C = 0.258$ and $\Gamma_{\rm M} = 1.0 \times 10^{-6}$.

Before studying how the induced gap affects the Kondo screening in the system, let us first analyze the Kondo effect in the absence of RSOI, and then see how it is modified by a finite RSOI. In Fig. 10, we show, in panel (a) the impurity entropy contribution $S_{\rm imp}$, and in panel (b) the magnetic moment $\mu^2_{\rm imp}$, both of them as a function of temperature ($10^{-8} < T < 1$), for $\lambda_R = 0.0$ and $0.025 \leqslant U \leqslant 0.175$. As expected, the characteristic behavior of the SIAM is observed as the temperature is lowered, namely, the crossovers from an FO fixed point to an LM fixed point, and then from LM to SC. Note that, for small values of U, such as $U = 0.025$ (black curve), the LM fixed point is not visible, as in this case

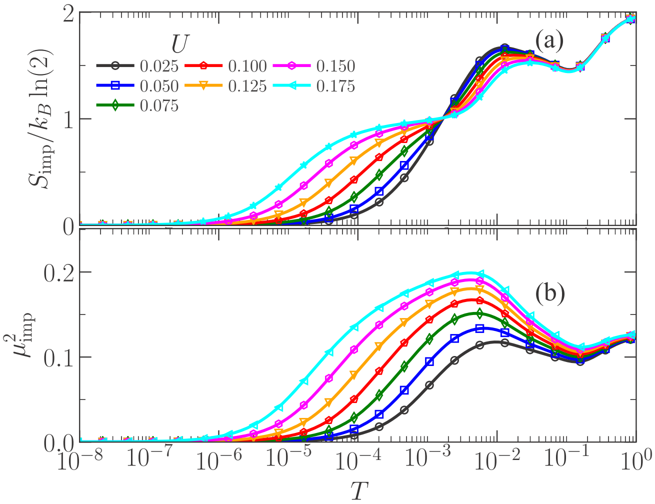

FIG. 10. (a) Impurity entropy $S_{\rm imp}$ and (b) magnetic moment $\mu^2_{\rm imp}$, for a metallic ($\lambda_R = 0.0$) 47-AGNR, as a function of temperature, for $0.025 \leqslant U \leqslant 0.175$, $V_C = 0.258$, and $\Gamma_{\rm M} = 1.0 \times 10^{-6}$.

the Kondo temperature becomes comparable to Γ and U, and the system is close to an intermediate valence situation. The intriguing small dip in the impurity magnetic moment, as well as in the entropy (presenting a small variation with U), for temperatures in the range 10^{-2}–10^{0}, points to the presence of van Hove singularities [72], coming from the quasi-one-dimensional (quasi-1D) band structure of the AGNR.

To see how the gap opening introduces the reentrant SIAM behavior, discussed in Sec. II, in Fig. 11 we repeat the calculations shown in Fig. 10, with the same set of parameters, except that λ_R is now finite, producing a gap $\Delta = 0.9 \times 10^{-5}$. For values of $U = 0.025$, up to $U = 0.075$, we clearly see, both from the impurity entropy $S_{\rm imp}$ [Fig. 11(a)] and from the impurity magnetic moment $\mu^2_{\rm imp}$ [Fig. 11(b)], the emergence of the reentrant SIAM behavior for temperatures below $\Delta \approx 10^{-5}$ (compare with the results in Fig. 10 for the same temperature range). As U increases, the Kondo temperature T_{K1} of the first Kondo screening decreases, so that the unstable LM fixed point becomes more pronounced (i.e., extends over a larger interval of temperature). As a consequence, the observed decrease of T_{K1}, as U increases, squeezes the first SC fixed point within a temperature range $\Delta \lesssim T \lesssim T_{K1}$, and, eventually, the first Kondo screening ceases to occur when T_{K1} becomes comparable to Δ. This is manifested in the progressive enhancement of $S_{\rm imp}$ and $\mu^2_{\rm imp}$ in this temperature region (because the first LM fixed point extends further down in temperature). It is interesting to observe that the reentrant Kondo temperature T_{K2} decreases much more rapidly than T_{K1} with increasing U, as observed in the fast increase of plateau extension of the reentrant LM fixed point. The decrease of T_{K1} with increasing U can be understood in terms of the Haldane expression for the Kondo temperature in the conventional SIAM [51]. From our calculations we find that the effective Coulomb repulsion $U_{\rm eff}$ increases by increasing U (not shown). Thus, even though the Haldane expression cannot be readily applied to obtain T_{K2}, it provides us with a good insight on why T_{K2} decreases rapidly by increasing U.

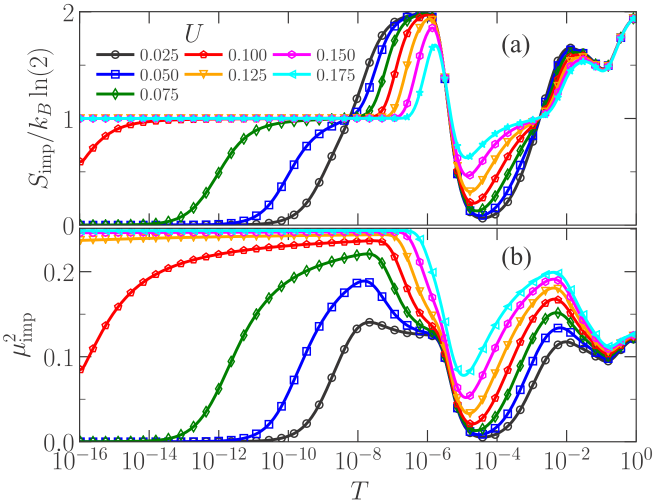

FIG. 11. (a) Impurity entropy $S_{\rm imp}$ and (b) magnetic moment $\mu^2_{\rm imp}$ for a 47-AGNR as a function of temperature, for fixed RSOI induced gap $\Delta = 0.9 \times 10^{-5}$, $\Gamma_{\rm M} = 1.0 \times 10^{-6}$, and different values of U.

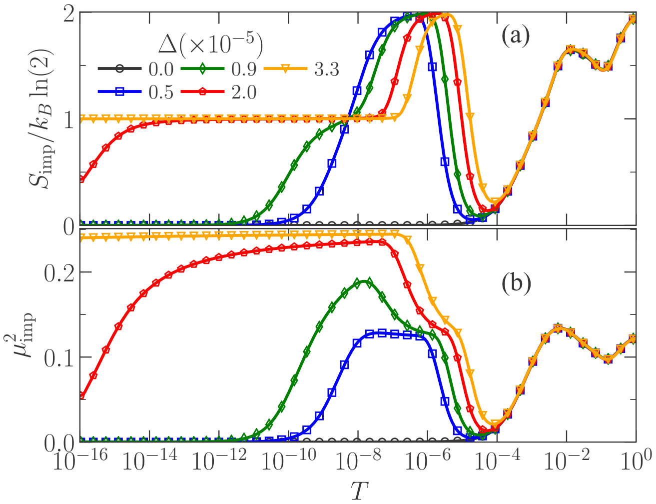

FIG. 12. (a) Impurity entropy $S_{\rm imp}$ and (b) magnetic moment $\mu^2_{\rm imp}$ for a 47-AGNR as a function of temperature, for different values of RSOI induced gap ($0.0 \leqslant \Delta \leqslant 3.3 \times 10^{-5}$). The parameter values for both panels are $\Gamma_{\rm M} = 1.0 \times 10^{-6}$ and $U = 0.05$.

Now, we proceed to a study of how the reentrant SIAM behavior is modified by changing the AGNR gap for a fixed U value. Figures 12(a) and 12(b) show, respectively, $S_{\rm imp}$ and $\mu^2_{\rm imp}$ as a function of T, for $U = 0.05$ and $0 \leqslant \Delta \leqslant 3.3 \times 10^{-5}$. After interpreting the results in Fig. 11, as just done above, where we fixed Δ and increased U, the results in Fig. 12 can be understood quite straightforwardly. Indeed, by increasing Δ, the extension of the first LM fixed point is squeezed from below, as $T_{K1} \approx 10^{-3}$ is now fixed (notice the collapse of all curves, in both panels, for $T \gtrsim 10^{-4}$), and the extent of the first SC fixed point is determined by Δ. In addition, the extension of the reentrant FO fixed-point plateau decreases for increasing Δ, indicating a decrease in the charge fluctuations in the reentrant SIAM for increasing

Δ. This suggests that the effective Coulomb repulsion $U_{\rm eff}$ associated to the reentrant SIAM increases with Δ, resulting in smaller T_{K2} values, which is clearly seen by the reentrant Kondo screening taking place at lower temperatures for larger Δ. Moreover, for $\Delta > T_{K1}$ (not shown), no Kondo screening takes place as Δ exceeds T_K (which is analogous to say that $\Gamma_c > \Gamma_0$) destroying the first Kondo stage, as discussed in Sec. II.

An important question, mainly for experimentalists, remains to be answered, namely, what are the estimated values for T_{K1} and T_{K2} for the AGNR + QI + STM system? Let us first present the highest T_{K2} value [blue open squares in Fig. 12(b)], where the Kondo temperature was obtained using Wilson's criterion, as done in Figs. 3(b) and 7(b). We assume realistic values for the model parameters, i.e., nearest-neighbor hopping $t \approx 2.7$ eV, which results in $D \approx 8.37$ eV, thus $2\Delta = 1.0 \times 10^{-5}D \approx 0.08$ meV, $U = 0.05D \approx 418$ meV, and $\Gamma_M = 1.0 \times 10^{-6}D \approx 8.37$ μeV. The NRG estimated values for T_{K1} and T_{K2} are approximately 106.72 K (9.2 meV) and 0.5 mK (0.043 μeV), respectively. Such a low value of T_{K2} (obtained for this set of parameters) would represent an obstacle to the experimental detection of the reentrant Kondo physics in the AGNR + QI + STM system. However, notice that we have a certain degree of flexibility in varying some of the parameters, like the AGNR width W, the RSOI λ_R (where both of them affect the Δ value), the coupling Γ_M of the STM-tip to the QI, as well as its Coulomb repulsion U. In addition, based on the understanding we gathered on the physics of the reentrant Kondo, we have some intuition on how to increase T_{K2}. Indeed, the semiconducting gap Δ is located between T_{K1} and T_{K2}, separated by a few orders of magnitude, i.e., $T_{K2} \ll \Delta \ll T_{K1}$, although there seems to be no restriction on how much T_{K2} may approach Δ, other than resulting in an unrealistically large T_{K1}, as both are strongly connected (see Fig. 6). From the results in the previous sections we know that T_{K2} should increase as $U_{\rm eff}$ decreases and $\Gamma_{\rm M}$ increases, with the former decreasing as U decreases. Following this recipe, but still using realistic parameter values, we manage to obtain $T_{K1} = 55.7$ K (4.8 meV) [73] and $T_{K2} = 10.2$ mK (0.9 μeV), by assuming $W \approx 11.56$ nm and $\lambda_R = 33.5$ meV (resulting in $2\Delta = 0.14$ meV), $\Gamma_M = 502$ μeV, and $U = 214$ meV. This T_{K2} value, we will argue below, is already much closer to being experimentally accessible.

To finish this section, without trying to exhaust the literature in the subject, we will place our results in the context of theoretical [43,74–77] and experimental [78–80] results that are related to the occurrence of consecutive Kondo effects (as one lowers temperature), dubbed in the literature, in general, as two-stage Kondo effects. There are two distinct flavors of it: (i) in QDs containing an even number of electrons, a singlet-triplet Kondo effect has been observed both in vertical QDs [81] as well as in lateral QDs [78], and, more recently, in carbon nanotube QDs [82]. Consecutive Kondo effects (dubbed as "two-stage Kondo effect") have been observed on both sides of the singlet-triplet transition in semiconducting QDs [78]. The effects have distinct mechanisms on each side of the transition, and both effects require the formation of an $S = 1$ state, with the presence of two screening channels on the triplet side and a single one on the singlet side. For example, in the singlet side, van der Wiel *et al.* [78] report values $T_{K1} \approx 3.5$ K (300 μeV) and $T_{K2} \lesssim 1$ K (86 μeV). (ii) In double-QD (DQD) systems, where one of the QDs (QD1) is embedded between the source and drain leads and the other QD (QD2) is side coupled to QD1, through a tunneling junction. In that case, for the right couplings between QD1 and the Fermi sea, and between both QDs, QD1 is Kondo screened first, at a higher temperature T_{K1}, by the Fermi sea electrons. At a much lower temperature T_{K2}, QD2 will be Kondo screened by the quasiparticles forming the Fermi-liquid ground state resulting from the first Kondo state. The spectral density that couples to QD2 is essentially the Kondo peak of QD1. This second flavor, although having a two-stage mechanism that is very diverse from the reentrant Kondo presented here, is more akin to our case since T_{K1} is, in general, orders of magnitude higher than T_{K2}. Therefore, the observation of its second stage has posed a stiff challenge to experimentalists. In that respect, it is interesting to note that Žitko [76], using NRG to simulate transport properties of a DQD system, has claimed that Sasaki *et al.* [80], doing measurements at low temperatures (in the range of few tens of mK), have actually observed fingerprints of the second (T_{K2}) Kondo stage. This illustrates the fact that, in our opinion, the proper use of gap engineering techniques in similar systems to our AGNR + QI + STM may result in the observation of the second Kondo stage described here.

IV. SUMMARY AND CONCLUSIONS

In summary, in this paper, using Anderson's PMS and NRG approaches, we have analyzed a system involving a QI strongly ($\Gamma_{\rm S}$) coupled to a semiconductor (defined by a gap 2Δ) and weakly ($\Gamma_{\rm M}$) coupled to a metal (Fig. 1). Our analysis has unveiled the existence of a sequence of two Kondo "stages": the first one, occurring at higher temperatures, is characterized by an unstable SC fixed point, defined by a Kondo temperature $T_{K1} > \Delta$ and associated to a Kondo screening that dissipates when $T \to \Delta$, from above. As already studied in detail in the literature (see Introduction), this unstable first-stage Kondo may not happen at all in case $\Gamma_0 = \Gamma_{\rm S} + \Gamma_{\rm M} < \Gamma_c$, as discussed at the beginning of Sec. II (see Fig. 2). In case it does happen, it will be followed, for $T \lesssim \Delta$, by a second-stage Kondo, characterized by a Kondo temperature $T_{K2} \ll T_{K1}$, that presents a *replica* of the usual SIAM-fixed-points sequence (FO → LM → SC), but for which, in contrast to the first-stage Kondo, the SC fixed point is now stable. We dub this "emergent" SIAM as *reentrant* effective SIAM, with an effective Hubbard $U_{\rm eff} \ll U$, which is clearly displayed as a peak in the impurity LDOS, alongside a second Kondo peak (see Fig. 5). The properties of both stages are thoroughly analyzed through the impurity's thermodynamic properties and LDOS, using NRG. The intuitive picture that emerges, after the analysis of the NRG results, is a simple one: the high-temperature first Kondo state develops through impurity screening by thermally excited semiconducting electrons, while the second stage involves screening by metallic electrons, once the semiconducting electrons are out of reach to thermal excitations ($T < \Delta$) and only the metallic (low) spectral weight inside the gap is available for impurity screening. In addition, in Sec. III, we propose a realistic system where the reentrant Kondo stage may possibly be experimentally observed: a magnetic impurity strongly coupled to an AGNR and weakly coupled to an STM tip. The proposal is based on the use of an electric-field-induced RSOI to tune a gap 2Δ in an otherwise metallic AGNR, and, through a full NRG analysis of this system, using realistic parameters, we show that both stages may be considered as experimentally accessible, as a recent theory work [76] has suggested that the second-stage Kondo, expected in DQD systems, has actually been observed [80] through charge transport measurements at low temperatures in a semiconducting DQD system. We hope that our findings may spur theory groups to apply other techniques to the analysis of this model, as well as study its charge transport properties, which is the preferred experimental tool for spectroscopic analysis of these mesoscopic systems. We also expect to motivate the proposal of additional systems that could be similarly modeled, involving not only carbon materials (as we have proposed), but also containing related materials that are amenable to appropriate gap engineering.

ACKNOWLEDGMENTS

It is a pleasure to acknowledge fruitful discussions with G. J. Ferreira. G.D. acknowledges an MS scholarship from the Brazilian agency Coordenação de Aperfeiçoamento de Pessoal de Nível Superior (CAPES), E.V. acknowledges support from Ohio University within the Robert Glidden Visiting Professorship program. Additional support from the Brazilian funding agencies CAPES and FAPEMIG is also acknowledged.

[1] P. W. Anderson, Science **177**, 393 (1972).

[2] J. Kondo, Prog. Theor. Phys. **32**, 37 (1964).

[3] A. C. Hewson, *The Kondo Problem to Heavy Fermions* (Cambridge University Press, Cambridge, 1993).

[4] D. Goldhaber-Gordon, H. Shtrikman, D. Mahalu, D. Abusch-Magder, U. Meirav, and M. Kastner, Nature (London) **391**, 156 (1998).

[5] P. W. Anderson, Phys. Rev. **124**, 41 (1961).

[6] H. R. Krishna-murthy, J. W. Wilkins, and K. G. Wilson, Phys. Rev. B **21**, 1003 (1980).

[7] R. Bulla, T. A. Costi, and T. Pruschke, Rev. Mod. Phys. **80**, 395 (2008).

[8] K. Takegahara, Y. Shimizu, and O. Sakai, J. Phys. Soc. Jpn. **61**, 3443 (1992).

[9] K. Takegahara, Y. Shimizu, N. Goto, and O. Sakai, Phys. B (Amsterdam) **186**, 381 (1993).

[10] T. Saso, J. Phys. Soc. Jpn. **61**, 3439 (1992).

[11] J. Ogura and T. Saso, J. Phys. Soc. Jpn. **62**, 4364 (1993).

[12] L. Cruz, P. Phillips, and A. H. Castro Neto, Europhys. Lett. **29**, 389 (1995).

[13] C. C. Yu and M. Guerrero, Phys. Rev. B **54**, 8556 (1996).

[14] K. Chen and C. Jayaprakash, Phys. Rev. B **57**, 5225 (1998).

[15] C. P. Moca and A. Roman, Phys. Rev. B **81**, 235106 (2010).

[16] M. R. Galpin and D. E. Logan, Phys. Rev. B **77**, 195108 (2008).

[17] M. R. Galpin and D. E. Logan, Eur. Phys. J. B **62**, 129 (2008).

[18] An alternate proposal could explore the *Mexican hat* electronic dispersion obtained in biased bilayer graphene, where the gap can be modified by an external electric field, as experimentally reported in E. V. Castro, K. S. Novoselov, S. V. Morozov, N. M. R. Peres, J. M. B. Lopes dos Santos, J. Nilsson, F. Guinea, A. K. Geim, and A. H. Castro Neto, Phys. Rev. Lett. **99**, 216802 (2007).

[19] J. Nygard, D. H. Cobden, and P. E. Lindelof, Nature (London) **408**, 342 (2000).

[20] P. Jarillo-Herrero, J. Kong, H. S. van der Zant, C. Dekker, L. P. Kouwenhoven, and S. De Franceschi, Nature (London) **434**, 484 (2005).

[21] K. Sengupta and G. Baskaran, Phys. Rev. B **77**, 045417 (2008).

[22] S.-P. Chao and V. Aji, Phys. Rev. B **83**, 165449 (2011).

[23] L. Fritz and M. Vojta, Rep. Prog. Phys. **76**, 032501 (2013).

[24] Z.-G. Zhu and J. Berakdar, Phys. Rev. B **84**, 165105 (2011).

[25] M. Kharitonov and G. Kotliar, Phys. Rev. B **88**, 201103(R) (2013).

[26] T.-F. Fang and Q.-f. Sun, Phys. Rev. B **87**, 075116 (2013).

[27] D. Mastrogiuseppe, A. Wong, K. Ingersent, S. E. Ulloa, and N. Sandler, Phys. Rev. B **90**, 035426 (2014).

[28] G.-Y. Li, T.-F. Fang, A.-M. Guo, and Q.-F. Sun, Phys. Rev. B **100**, 115115 (2019).

[29] P. Haase, S. Fuchs, T. Pruschke, H. Ochoa, and F. Guinea, Phys. Rev. B **83**, 241408(R) (2011).

[30] A. K. Mitchell and L. Fritz, Phys. Rev. B **88**, 075104 (2013).

[31] D. May, P.-W. Lo, K. Deltenre, A. Henke, J. Mao, Y. Jiang, G. Li, E. Y. Andrei, G.-Y. Guo, and F. B. Anders, Phys. Rev. B **97**, 155419 (2018).

[32] Y. Jiang, P.-W. Lo, D. May, G. Li, G.-Y. Guo, F. B. Anders, T. Taniguchi, K. Watanabe, J. Mao, and E. Y. Andrei, Nat. Commun. **9**, 2349 (2018).

[33] L. Li, Y.-Y. Ni, Y. Zhong, T.-F. Fang, and H.-G. Luo, New J. Phys. **15**, 053018 (2013).

[34] J. Ren, H. Guo, J. Pan, Y. Y. Zhang, X. Wu, H.-G. Luo, S. Du, S. T. Pantelides, and H.-J. Gao, Nano Lett. **14**, 4011 (2014).

[35] J.-H. Chen, L. Li, W. G. Cullen, E. D. Williams, and M. S. Fuhrer, Nat. Phys. **7**, 535 (2011).

[36] V. G. Miranda, L. G. G. V. Dias da Silva, and C. H. Lewenkopf, Phys. Rev. B **90**, 201101(R) (2014).

[37] C. A. Büsser, G. B. Martins, and A. E. Feiguin, Phys. Rev. B **88**, 245113 (2013).

[38] D. Krychowski, J. Kaczkowski, and S. Lipinski, Phys. Rev. B **89**, 035424 (2014).

[39] Y. Li, A. T. Ngo, A. DiLullo, K. Z. Latt, H. Kersell, B. Fisher, P. Zapol, S. E. Ulloa, and S.-W. Hla, Nat. Commun. **8**, 946 (2017).

[40] G. S. Diniz, G. I. Luiz, A. Latgé, and E. Vernek, Phys. Rev. B **97**, 115444 (2018).

[41] K. Wakabayashi, Y. Takane, M. Yamamoto, and M. Sigrist, New J. Phys. **11**, 095016 (2009).

[42] P. W. Anderson, J. Phys. C: Solid State Phys. **3**, 2436 (1970).

[43] P. S. Cornaglia and D. R. Grempel, Phys. Rev. B **71**, 075305 (2005).

[44] R. Žitko, NRG Ljubljana: open source NRG code available at http://nrgljubljana.ijs.si.

[45] As will be more clearly explained later, what we call T_K in this section will become T_{K1}, once we introduce a finite $\Gamma_{\rm M}$ to

the calculations. However, in this section, to avoid confusion, we will refer to the ($\Gamma_M = 0$) PMS Kondo temperature simply as T_K.

[46] J. R. Schrieffer and P. A. Wolff, Phys. Rev. **149**, 491 (1966).

[47] Equivalently, we could also choose to look for a critical Δ_c for a given $J_S^{(0)}$.

[48] We have used the fact that $\rho_S(D) = \rho_0 = 1/2\sqrt{D^2-\Delta^2}$, which, for $\Delta = 0$, results in $\rho_0 = 1/2D$.

[49] D. N. Zubarev, Phys. Usp. **3**, 320 (1960).

[50] J. H. Jefferson, J. Phys. C: Solid State Phys. **10**, 3589 (1977).

[51] F. D. M. Haldane, Phys. Rev. Lett. **40**, 416 (1978).

[52] M. Cheng and K. Ingersent, Phys. Rev. B **87**, 075145 (2013).

[53] M. Cheng, T. Chowdhury, A. Mohammed, and K. Ingersent, Phys. Rev. B **96**, 045103 (2017).

[54] S. Massidda, A. Continenza, A. J. Freeman, T. M. de Pascale, F. Meloni, and M. Serra, Phys. Rev. B **41**, 12079 (1990).

[55] A. J. Heeger, S. Kivelson, J. R. Schrieffer, and W. P. Su, Rev. Mod. Phys. **60**, 781 (1988).

[56] S. Borghardt, J.-S. Tu, F. Winkler, J. Schubert, W. Zander, K. Leosson, and B. E. Kardynał, Phys. Rev. Mater. **1**, 054001 (2017).

[57] L. Lenz, D. F. Urban, and D. Bercioux, Eur. Phys. J. B **86**, 502 (2013).

[58] Depending on the number of dimmers along the transverse direction, the AGNR can be metallic or an *intrinsic* semiconductor. In what follows, we will explore the extrinsic tunable induced gap in metallic AGNR by means of an external agent.

[59] V. M. Pereira, A. H. Castro Neto, and N. M. R. Peres, Phys. Rev. B **80**, 045401 (2009).

[60] A. H. Castro Neto, F. Guinea, N. M. R. Peres, K. S. Novoselov, and A. K. Geim, Rev. Mod. Phys. **81**, 109 (2009).

[61] C. L. Kane and E. J. Mele, Phys. Rev. Lett. **95**, 226801 (2005).

[62] M. Zarea and N. Sandler, Phys. Rev. B **79**, 165442 (2009).

[63] M. B. Nardelli, Phys. Rev. B **60**, 7828 (1999).

[64] M. P. L. Sancho, J. M. L. Sancho, and J. Rubio, J. Phys. F: Met. Phys. **14**, 1205 (1984).

[65] Thus, the hybridization function just described is equivalent to the $\Gamma_0 = \Gamma_S + \Gamma_M$ hybridization function defined in Sec. II.

[66] Co adatoms, deposited on monolayer graphene [deposited, in turn, over a SiC (0001) substrate], have shown to be most favorable in a top-site configuration (see Fig. 8), as experimentally reported by T. Eelbo, M. Waśniowska, P. Thakur, M. Gyamfi, B. Sachs, T. O. Wehling, S. Forti, U. Starke, C. Tieg, A. I. Lichtenstein, and R. Wiesendanger, Phys. Rev. Lett. **110**, 136804 (2013).

[67] D. O. Demchenko, A. V. Joura, and J. K. Freericks, Phys. Rev. Lett. **92**, 216401 (2004).

[68] E. I. Rashba, Phys. Rev. B **79**, 161409(R) (2009).

[69] Y. S. Dedkov, M. Fonin, U. Rüdiger, and C. Laubschat, Phys. Rev. Lett. **100**, 107602 (2008).

[70] A. Varykhalov, D. Marchenko, M. R. Scholz, E. D. L. Rienks, T. K. Kim, G. Bihlmayer, J. Sánchez-Barriga, and O. Rader, Phys. Rev. Lett. **108**, 066804 (2012).

[71] D. Marchenko, A. Varykhalov, M. R. Scholz, G. Bihlmayer, E. I. Rashba, A. Rybkin, A. M. Shikin, and O. Rader, Nat. Commun. **3**, 1232 (2012).

[72] The van Hove singularities are fixed for a given λ_R, however, as λ_R is varied (for the range of λ_R considered), the first peak is strongly modified, as one can note in Fig. 9.

[73] Note that the AGNR used for these calculations had a width ($W \approx 11.56$ nm) different from the one used for the calculations in Fig. 12 ($W \approx 5.65$ nm). This resulted in a Γ_S (not shown) considerably smaller than the one obtained for the AGNR in Fig. 12, thus a smaller T_{K1} than the one expected from just a decrease in U.

[74] M. Pustilnik and L. I. Glazman, Phys. Rev. Lett. **87**, 216601 (2001).

[75] W. Hofstetter and G. Zarand, Phys. Rev. B **69**, 235301 (2004).

[76] R. Žitko, Phys. Rev. B **81**, 115316 (2010).

[77] I. L. Ferreira, P. A. Orellana, G. B. Martins, F. M. Souza, and E. Vernek, Phys. Rev. B **84**, 205320 (2011).

[78] W. G. van der Wiel, S. De Franceschi, J. M. Elzerman, S. Tarucha, L. P. Kouwenhoven, J. Motohisa, F. Nakajima, and T. Fukui, Phys. Rev. Lett. **88**, 126803 (2002).

[79] G. Granger, M. A. Kastner, I. Radu, M. P. Hanson, and A. C. Gossard, Phys. Rev. B **72**, 165309 (2005).

[80] S. Sasaki, H. Tamura, T. Akazaki, and T. Fujisawa, Phys. Rev. Lett. **103**, 266806 (2009).

[81] S. Sasaki, S. De Franceschi, J. M. Elzerman, W. G. van der Wiel, M. Eto, S. Tarucha, and L. P. Kouwenhoven, Nature (London) **405**, 764 (2000).

[82] P. Petit, C. Feuillet-Palma, M. L. Della Rocca, and P. Lafarge, Phys. Rev. B **89**, 115432 (2014).